Zhukov, S. S.; Zhukova, E. S.; Melentev, A. V.; Gorshunov, B. P.; Tsapenko, A. P.; Kopylova, D. S.; Nasibulin, Albert G.

Terahertz-infrared spectroscopy of wafer-scale films of single-walled carbon nanotubes treated by plasma

Published in:
Carbon

DOI:
10.1016/j.carbon.2021.12.076

Published: 15/04/2022

Document Version
Peer-reviewed accepted author manuscript, also known as Final accepted manuscript or Post-print

Terahertz-infrared spectroscopy of wafer-scale films of single-walled carbon nanotubes treated by plasma

S.S.Zhukov[1*], E.S.Zhukova[1], A.V.Melentev[1], B.P.Gorshunov[1]

[1]*Laboratory of Terahertz Spectroscopy, Center for Photonics and 2D Materials, Moscow Institute of Physics and Technology (National Research University), Dolgoprudny, Russia*

A.P.Tsapenko[2], D.S.Kopylova[2], Albert G. Nasibulin[2,3]

[2] *Skolkovo Institute of Science and Technology, Nobel str. 3, Moscow, 143026, Russia*

[3] *Aalto University, Department of Chemical Engineering, 00076, Aalto, Finland*

Keywords: Carbon Nanotubes, Thin Films, Plasma Treatment, Terahertz Spectroscopy, Temperature Coefficient of Resistance

Abstract

We investigated terahertz-infrared electrodynamic properties of wafer-scale films composed of plasma-treated single-walled carbon nanotubes (SWCNTs) and films comprising SWCNTs grown with different lengths. The spectra of complex conductance of the films were measured at frequencies 5-20 000 cm^{-1} and in the temperature interval 5-300 K. Terahertz spectral response of films of pristine SWCNTs is well described with the Drude conductivity model and a plasmon resonance located at ≈100 cm^{-1}. Stepwise treatment of the films with oxygen plasma led to a gradual suppression of the Drude spectral weight from the low-frequency side. For films with the nanotubes shorter than 1 μm, *i.e.*, close to electrons mean free path and localization length, scattering of charge carriers at the nanotubes edges is shown to additionally contribute to the carriers scattering rate and to the damping of plasmon resonance. The temperature coefficient of ac resistance (ac TCR) in both kinds of films is found to strongly increase in amplitude during cooling and frequency decrease. The values of ac TCR increase in films with longer time of plasma treatment and nanotubes with shorter length but reach saturation in films with exposure time longer than ≈100 s or composed from SWCNTs shorter than 1 μm.

* Corresponding author. Tel: +7-498-744-6538. e-mail address: ssz1978@gmail.com

Graphical abstract

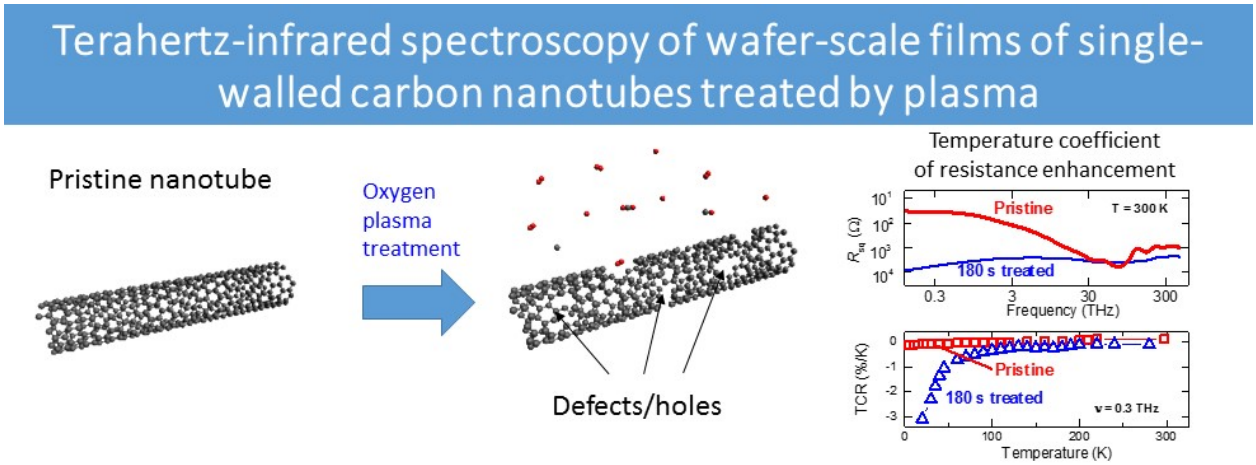

1.Introduction

Among the existing carbon nanomaterials and nanostructures, a particular interest is devoted to wafer-scale films comprising a network of randomly oriented single-walled carbon nanotubes (SWCNTs). Such films possess a remarkable combination of physical and chemical properties - enormous mechanical stability, large effective surface-to-volume ratio, stretchability and flexibility, low weight (compared to metallic analogs), high adhesion to various substrates, chemical inertness, exceptional electrical and optical properties. In addition to that, large (tens of square centimeters) and thin (down to a few nanometers) free-standing films can be easily manufactured by inexpensive methods, making such networks very promising for designing various electronic devices and elements, like transparent electrical conductors and electrodes, coatings and electromagnetic shields, polarizers, modulators, reflectors, and antennas. Appropriate characteristics are provided by pronounced metallicity of high-quality networks of pristine or doped SWCNTs, with their dc and ac (microwave, terahertz, far-infrared) electrodynamics mostly governed by delocalized charge carriers that can freely travel within separate nanotubes and relatively easily overcome (tunnel or hop over) potential barriers at nanotubes' intersections [1–7]. Additional prospects for using the SWCNTs in electronics are opened up by specific enhancement and tuning of their performance, e.g., with chemical or laser treatment [8,9] or exposure to plasma [10]. Though such treatment can reduce the metallicity of SWCNTs, they acquire additional functionalities due to defect sites/states or chemical functional groups generated at their walls [10–12] that can be used for the fabrication of chemical and biological sensors, radiation generators, detectors, polarizers and modulators, for conductance control in SWCNT-based field-effect transistors [2,13–16]. For example, we have recently shown that exposure of SWCNT films to oxygen plasma allows fine-tuning of their electronic properties, in particular, enhancing the temperature coefficient of resistance (TCR) in

comparison with that of pristine SWCNTs, and reaching high sensitivity, short response time, smooth spectral characteristics and low noise level of infrared bolometers [10].

In order to make the most efficient use for potential applications of the properties of networks of pristine or treated SWCNTs, detailed knowledge is needed of the mechanism of electrical charges dynamics, the character of their interaction with defects introduced by various treatments and of the nature of these defects states. Terahertz-infrared (THz-IR) spectroscopy is an excellent method to obtain relevant information. This contactless technique has been successfully applied in [5,6] to characterize charge transport mechanisms of wafer-scale films of high-quality pristine and doped (with I, CuCl, $AuCl_3$) SWCNTs. It was shown that the THz-IR electrodynamic response of the films is almost fully dominated by unbound charge carriers with a weak gap-like feature detected in the spectra below 0.3 THz. This feature appears due to energy barriers experienced by the carriers at the intersections between SWCNTs. The barriers lead to a partial localization of carriers that manifests as a relatively weak (spectral weight significantly smaller than that of the free-carrier Drude component) plasmon-like excitation located around 100 cm^{-1}. A similar approach was utilized in [17–19] to characterize THz-IR spectra of thin films of SWCNTs of different average lengths; the authors claimed that the THz response of the films is of plasmonic nature and can be described with the model of the localized plasmon resonance.

Here, we present the results of the first studies of an influence of oxygen plasma treatment on the THz-IR electrodynamics of wafer-scale films comprising SWCNTs. We show that while the THz-IR response of pristine films is nearly fully determined by quasi-free charge carriers, a stepwise exposure of the films to oxygen plasma results in gradually increasing etching away of the sub-terahertz spectral weight in the conductance spectra with a corresponding decrease of the dc conductance. The observed changes are interpreted on a phenomenological level and are related to the appearance of defects induced by plasma treatment, holes, and chemical functional groups at the nanotube walls that create additional scattering centers and potential barriers for carriers on their pathways which lead to progressively increasing scattering and localization of the carriers. Based on the THz-IR experiments performed on films made of SWCNTs of different lengths, we show that the effect of plasma treatment on the electrodynamics of the films is qualitatively similar to that observed in the films with a shorter average length of SWCNTs within the films. The temperature coefficient of resistance of both kinds of films is analyzed.

2.SWCNT films preparation and characterization

The SWCNT films for plasma treatment (duration up to 420 s, power of 100 W, and pressure of 0.3 mbar) were synthesized by an aerosol CVD method, based on ferrocene vapor decomposition

in the atmosphere of carbon monoxide, and deposited on a nitrocellulose filter in the form of individual and small diameter bundles. After that, the films were dry-transferred onto metallic rings with a clear aperture ≈10 mm and utilized in spectroscopic experiments in a free-standing form. Films with different lengths of SWCNTs (0.3, 1, 6, and 13 μm) were synthesized by varying the experimental conditions (temperature and CO concentration), as described in [20] where also the SWCNT's length distribution in various films is analyzed. For spectroscopic measurements they were deposited on a 5 μm thick polyethylene (PE) substrate that is transparent for THz and IR radiation. The average nanotube lengths were determined by transmission and scanning electron microscopy (Philips CM200 FEG and JEOL JSM-7500F). The SWCNT network morphology was also studied by atomic force microscopy (Veeco Dimension 5000, Veeco Instruments). The transmission electron microscopy (TEM) and scanning electron microscopy (SEM) images of the pristine and plasma treated films are presented in Figure 1 (a) and (b), respectively. It is clearly seen that the oxygen plasma treatment does not change the morphology of the SWCNTs. Exposure to plasma introduces a large number of defects in the walls of carbon nanotubes, as is mostly pronounced in TEM images. In the right image on in (a) panel, there are metallic catalytic particles in the edges of nanotubes. These particles remain almost intact after the plasma treatment but become covered by several layers of probably metal carbide (left image in (a)) [10]. The particles are seen more clearly also on SEM images of treated samples (b) due to etching of large amount of carbon nanotubes in plasma. The plasma treatment causes appearance of large number of structural defects with subsequent oxidation. This was confirmed by XPS analysis in our previous work [10]. The oxidation leads to the appearance of carboxy, hydroxy, epoxy and carbonyl functional groups on the defects. The analysis also showed the increase of number sp3- hybridized C atoms associated with defectiveness compared to pristine nanotubes which are mainly consist of sp2-hybridized carbon.

We determined the spectra of real and imaginary parts of complex conductivity $\sigma^*(\nu,T) = \sigma_1(\nu,T) + i\sigma_2(\nu,T)$ and of complex dielectric permittivity $\varepsilon^*(\nu,T) = \varepsilon'(\nu,T) + i\varepsilon''(\nu,T)$ of the films from the spectra of complex (amplitude and phase) transmission coefficient measured with the TeraView time-domain spectrometer at frequencies in the range from $\nu \approx 5$ cm^{-1} up to $\nu \approx 100$ cm^{-1}. The spectra of transmission coefficients $Tr(\nu,T)$ of the samples in the infrared range were measured using the Bruker Fourier-transform spectrometer Vertex 80V. The home-made and commercial optical helium-flow cryostats were used to examine the materials in the temperature interval T=5 – 300 K. All measurements were performed in transmission mode, as shown in Figure 1(c). Broadband THz-IR spectra of electrodynamic response (complex

permittivity and conductivity) of the films were obtained by a combined analysis of THz and IR data as described below.

(a)

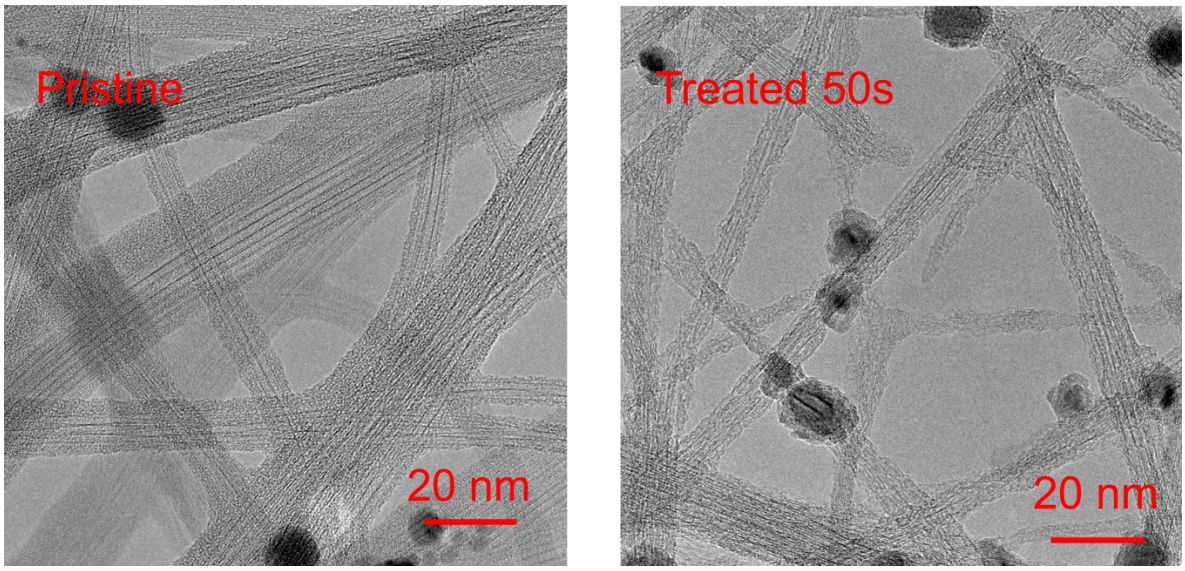

(b)

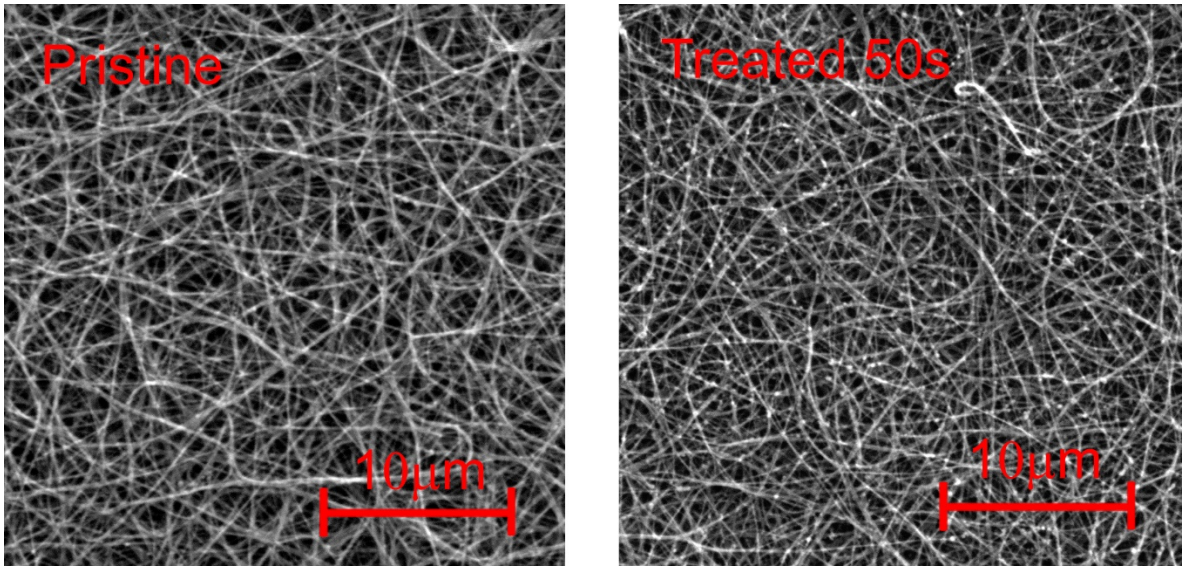

(c)

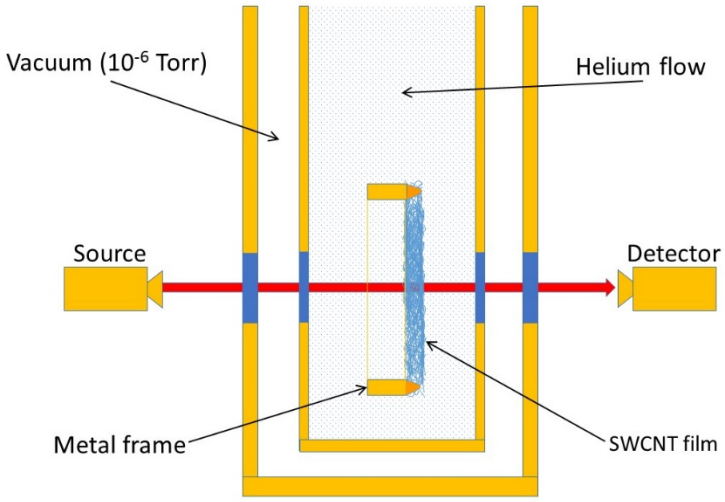

Figure 1. (a,b) Microscopic characterization of pristine and plasma-treated carbon nanotubes films by (a) Transmission Electron Microscopy (TEM) and (b) Scanning Electron Microscopy (SEM). (c) Scheme used for measurements of temperature-dependent spectra of terahertz complex conductance and infrared transmission. For terahertz and infrared experiments commercial TeraView time-domain spectrometer and Fourier-transform Bruker Vertex 80V spectrometer were used.

3.Results and discussion

In Fig.2 we show the spectra of transmission coefficients and real and imaginary parts of conductance of films with plasma-treated SWCNTs and composed of SWCNTs with different lengths. In the infrared region, above 3000 cm^{-1}, distinct minima in transmissivity and the peaks in conductance spectra are observed, which are related to the well-known interband transitions between 1D van Hove singularities [21]. The wavy structure between 200 and 2000 cm^{-1} in Fig.2a is connected with the Fabry-Perot effect, *i.e.*, interference of radiation within PE film. At lower far-infrared (FIR) and THz frequencies, the transmission coefficient spectra of both kinds of films look similar and show gradual growth after exposure to plasma and in films with shorter nanotubes length. We first analyze the spectra obtained for SWCNT films with different lengths.

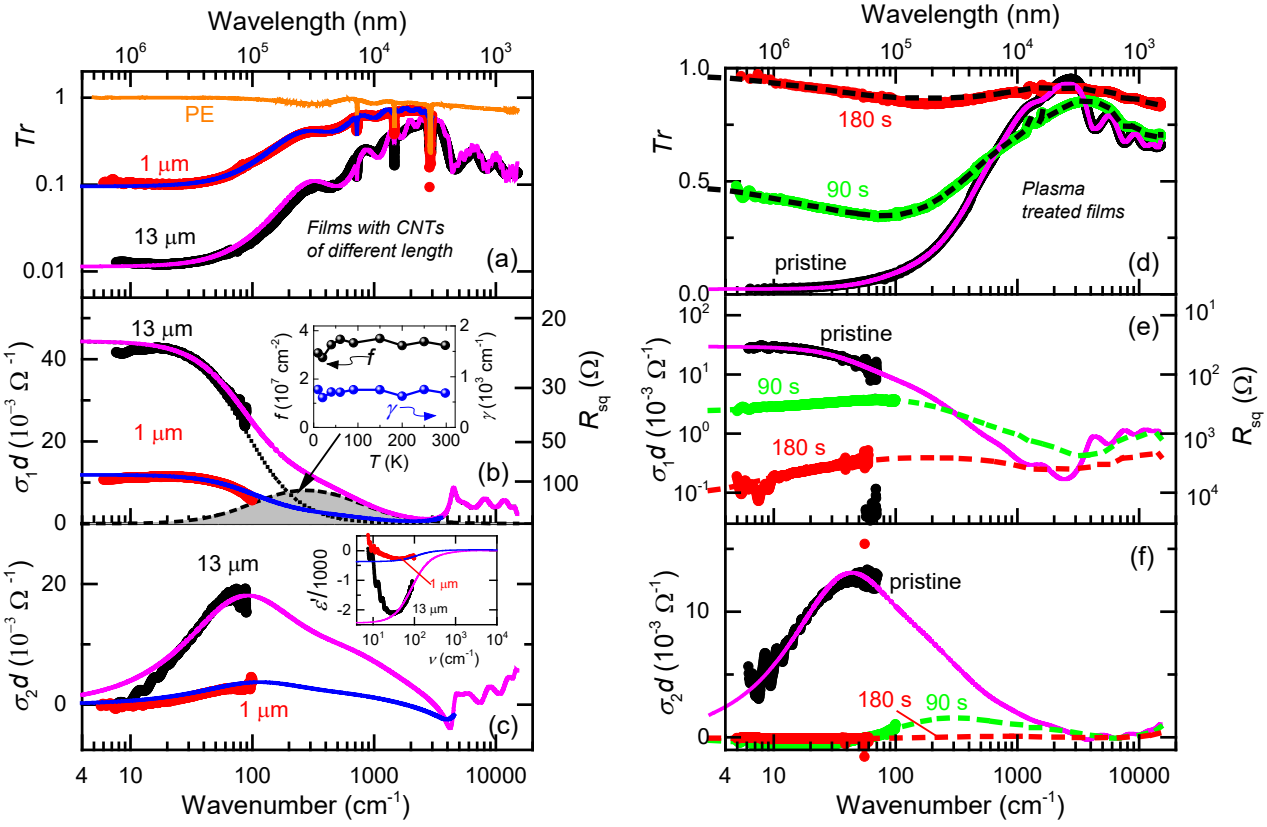

Fig.2. Panels a-c: Room-temperature terahertz-infrared spectra of transmission coefficient (a), effective real conductance and surface resistance (b), and effective imaginary conductance (c) of SWCNT films composed of SWCNTs with two different average lengths (1 μm and 13 μm) on a 5 μm thick polyethylene substrate. Dots correspond to directly measured spectra, lines – least-square fitting results with the Drude model describing free carriers' response and Lorentzians modeling infrared interband transitions and terahertz plasmon resonance, as described in the text. The transmission coefficient spectrum of the PE substrate is shown by the orange line on panel (a). The grey-shaded area in panel (b) shows the absorption band due to plasmon resonance for the film with 13 μm long SWCNTs; the dotted line corresponds to fitting when the plasmon band is not taken into account. Inset in (b): temperature dependence of parameters of plasmon resonance – damping γ and oscillator strength f. Inset in (c): spectra of the real part of permittivity of the two films (calculated assuming films with thickness 100 nm) with corresponding fits. Panels d-f: Room-temperature terahertz-infrared spectra of transmission coefficient (d), effective real conductance and surface resistance (e), and effective imaginary conductance (f) of free-standing SWCNT films composed of pristine SWCNTs (black color) and of SWCNTs treated with the plasma during 90 s (green color) and 180 s (red color). Dots correspond to directly measured conductance spectra; the solid lines for pristine film indicate least-square fitting results with the Drude model (Eq2) describing free carriers response and Lorentzians (Eq1) modeling infrared interband transitions and terahertz plasmon resonance. As discussed in the text, for plasma-treated films, the Drude fit was not possible, and the terahertz spectra were modeled with an artificial Lorentzians contribution; the so-obtained spectra of $\sigma_1 d$ and $\sigma_2 d$ are shown with dashed lines.

Due to the high porosity of the films, their boundaries cannot be specified precisely. Therefore, we discuss our results without assigning a certain thickness to any of the films and

without specifying their internal structure, as we did in [5,6]. For that, we use the model of a complex conducting surface developed in [22] for thin conducting layers. The frequency-temperature dependent complex conductance of such layer is given by $Y(\nu,T) = \sigma_1(\nu,T)*d + i\sigma_2(\nu,T)*d$, where σ_1 and σ_2 are the real and imaginary parts of the layer conductivity and d is its thickness if the layer is homogeneous. We obtain spectra of real and imaginary conductances of SWCNT films shown in Fig.2b,c by least-square processing of the transmission coefficient spectra. The expression for the transmission coefficient of a two-layer system (PE substrate and SWCNT film) is given in [23]. Here we process the spectra of transmission coefficients together with directly measured real and imaginary THz conductances using the same method as was previously employed in papers [5,6]. Minima in transmissivity above ≈3000 cm^{-1} are modeled with regular Lorentzian expression that is written for dielectric permittivity as

$$\varepsilon^*(\nu) = \varepsilon'(\nu) + i\varepsilon''(\nu) = \frac{f}{\nu_0^2 - \nu^2 + i\nu\gamma}, \quad (1)$$

where $f=\Delta\varepsilon\nu_0^2$ is the oscillator strength, $\Delta\varepsilon$ is the dielectric strength (dielectric contribution), ν_0 is the resonance frequency, and γ is the damping factor. Lower-frequency spectra are determined by delocalized charge carriers and are modeled with the Drude expression for the complex conductivity [24,25]:

$$\sigma*(\nu)\cdot d = \sigma_1(\nu)\cdot d + i\sigma_2(\nu)\cdot d = \left(\frac{\sigma_{dc}\gamma_D}{\gamma_D^2 + \nu^2} + i\frac{\sigma_{dc}\nu\gamma_D}{\gamma_D^2 + \nu^2}\right)\cdot d, \quad (2)$$

where σ_{dc} is the dc conductivity, and γ_D is the charge-carrier scattering rate. In order to consistently describe the transmissivity and conductance spectra, we had to introduce an additional term in the form of an absorption band located around 100 cm^{-1} (shaded area in Fig.2b) that is modeled with the Lorentzian expression (1). The band corresponds to the plasmonic resonance of charge carriers that are partly confined by potential barriers at the intersections of SWCNTs [5,6]. According to the inset in Fig.2b, the parameters of the band are practically independent of the temperature, which is in agreement with the results of [5,6]. The response of films with relatively long (13 μm) SWCNTs is well described by the Drude conductivity model above 30-40 cm^{-1}; here, the real part of THz permittivity attains large negative values [inset in panel (c)] - typical signature of metallic response. Deviations from the Drude behavior below 30-40 cm^{-1} [see also the inset in panel (c)] are discussed below. When the nanotube's length becomes shorter, strong "deformation" of the films' Drude-type spectral response is observed, which is seen as an overall decrease of the real and imaginary parts of THz conductance and of the absolute value of real THz permittivity. Corresponding evolution of the THz real conductance spectra are shown in more detail in Fig.3: a broad peak progressively

develops in the spectra and shifts to higher frequencies, finally above 100 cm^{-1} for the film with 0.3 μm long SWCNTs. Similar behavior was detected in the studies of the dependence of THz conductivity on the SWCNT length in [18] and also obtained from calculations based on Waterman–Truell formula in [19].

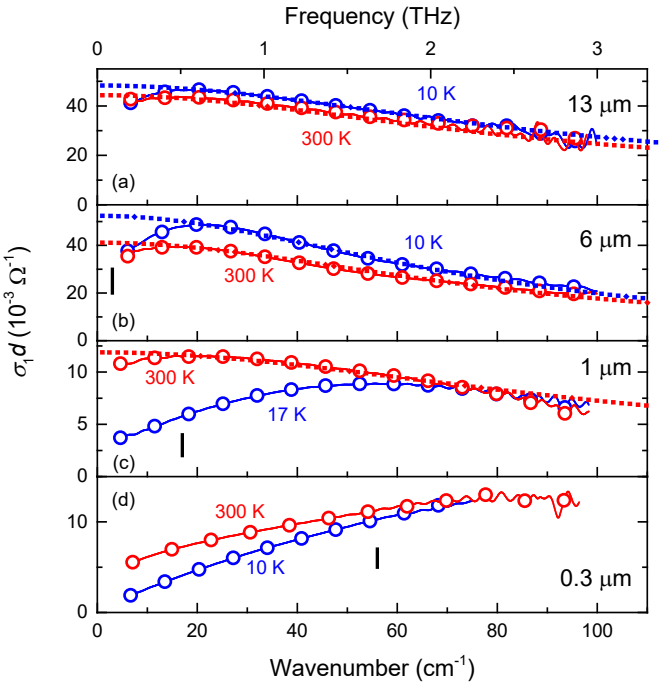

Fig.3. Terahertz spectra of the real part of conductance of SWCNT films composed of SWCNTs with different average lengths as indicated, measured at two different temperatures. Dots+lines show experimental data, dotted lines in panels (a,b,c) indicate results of least-square fitting of spectra of SWCNT films using the Drude conductivity model (2) to describe the response of delocalized carriers and Lorentzian expression (1) to describe plasmon resonance at around 100 cm^{-1}. Such fitting is not possible at low temperatures for films composed of SWCNTs of 1 μm length and at all temperatures for the films consisting of SWCNTs with a 0.3 μm average length, as described in the text. Vertical bars indicate the roughly estimated values of crossover frequencies ν_{co} below which deviations from Drude-like response are expected, as discussed in the text.

We qualitatively interpret the observed phenomena basing on our earlier findings [6], considering three features that determine the THz-IR electrodynamics of SWCNT films: (a) contribution from delocalized carriers described by the Drude conductivity model; (b) relatively weak absorption band around 100 cm^{-1} connected with plasmonic oscillations of carriers localized between intersections of SWCNTs in the films; (c) a gap-like feature at or below ≈10 cm^{-1} (0.3 THz) caused by tunnel barriers, experienced at low temperatures by the carriers at the SWCNTs' contacts. All these mechanisms manifest themselves in the spectra of the film with 13 μm long nanotubes. The observed progressing etching of the low-frequency part of the real THz conductance spectral weight in the films with shorter nanotubes can be qualitatively understood by assuming increasing partial localization of charge carriers between the edges of SWCNTs in

shorter SWCNTs. At high temperatures, the thermal energy k_BT (k_B is the Boltzmann constant) is large enough to assist carriers to overcome potential barriers created by such edges so that the response is Drude-like. In contrast, at low temperatures, the carriers get stuck in-between, with a corresponding decrease of the low-frequency conductance, see Fig.3c,d. The crossover frequency ν_{co}, below which deviations from the Drude response should be observed, can be roughly estimated as $\nu_{co} \approx v_F(2L)^{-1}$ where v_F is the Fermi velocity and L is the nanotube length. It is assumed here that if during half-period $(2\nu)^{-1}$ of the probing electromagnetic radiation (*i.e.*, when the electric field vector is pointing in one direction) the charge carrier travels the distance $v_F*(2\nu)^{-1}<L$ that is shorter than the nanotube length, it will not "feel" the localizing barriers and respond Drude-like. The inverse proportionality to the SWCNT length of the peak frequency in the THz conductance spectra (that is supposed to be related to ν_{co}) was observed experimentally and also follows from the Monte Carlo simulations of the dynamical response of charges located within 1D metallic "boxes" [18]. The values of ν_{co} obtained with the Fermi velocity $v_F \approx 10^8$ cm/s [26] are indicated by vertical bars in Fig.3b,c,d and correlate well with the maxima in the room-temperature real conductance spectra; at low temperatures, additional suppression of the THz conductance seen at frequencies $\nu > \nu_{co}$ can be caused by tunnel energy gaps.

The above oversimplified qualitative considerations agree with the predictions of more rigorous theoretical models developed for linear conducting chains of variational lengths and one-dimensional disordered lattices [27–29]. It had been shown in the referred papers that at high enough temperatures and/or frequencies when charge carriers localization effects are not dominant, the electrodynamics of such systems can be described by the Drude formalism with nearly frequency-independent conductivity and permittivity at frequencies significantly lower than scattering rate, $\nu << \gamma_D$. In the opposite case, localization of carriers leads to suppression of the low-frequency conductivity that grows with frequency as $\sigma_1 \sim \nu^s$ ($s<1$) following the Mott's hopping conduction concepts [30,31].

In Fig.4 we present the obtained dependences of the Drude condensate and plasmonic resonance parameters on the nanotube length. For films with SWCNT lengths in the range 1-13 μm, the Drude scattering rate of charge carriers γ_D=50-80 cm^{-1} remains practically unchanged and close to that in films with pristine SWCNTs [5,6]. The scattering rate shows a strong increase for films with L=0.3 μm. The closeness of this value to the carriers' mean free path (0.05-0.1 μm) and localization length (≈0.4 μm) [6] means that for films with L<1 μm, the additional scattering of carriers at nanotubes edges becomes essential. Decrease of the dc conductance in films with shorter SWCNTs should be attributed to both strengthening of the scattering process and a certain reduction of free carrier's concentration due to their growing involvement in the plasmonic oscillations. This is evidenced by the noticeable increase of

spectral weight f of the plasmon resonance, see Fig.4b. Note that the growth of the plasmon oscillator strength is strongest again in films with SWCNTs length L<1 μm, when the length of the nanotubes becomes comparable with plasmon localization length. According to Fig.4c, the scattering of carriers on SWCNT edges contributes also to the damping of plasmonic oscillations characterized by the damping factor γ. The position of the plasmonic resonance f_0 shifts to high frequencies for shorter SWCNTs, in accordance with theoretical expectations giving $f_0=v_p(\pi L)^{-1}$ where $v_p\approx 4v_F$ is the plasmon velocity [32].

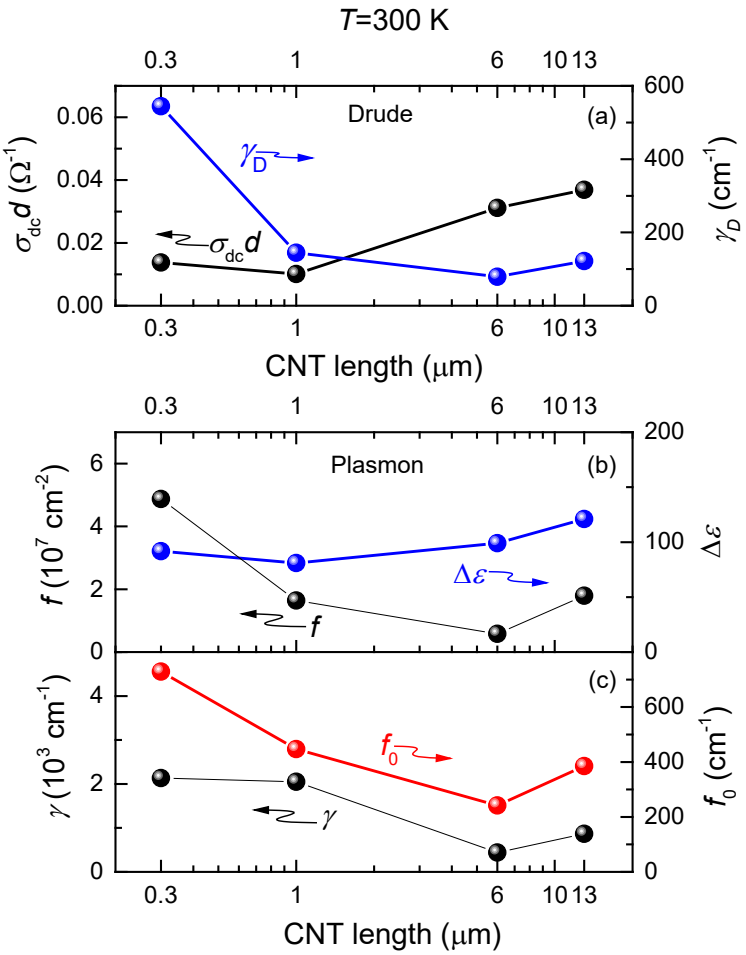

Fig.4. Dependence on SWCNTs' average length of effective parameters, dc conductance $\sigma_{dc}d$ and scattering rate γ_D, Eq. (2), of quasi-free charge carriers in the SWCNT films (a) and of parameters of plasmon excitation, oscillator strength f, dielectric strength $\Delta\varepsilon$, damping γ, and frequency f_0, Eq1 (b,c).

We now consider the results obtained for plasma-treated SWCNT films. From Fig.2d,e,f, and Fig.5, it is seen that exposure to plasma leads to the changes in the transmissivity and complex conductance spectra of the films that look similar to those observed for films with variable SWCNT length. It was not possible, however, to apply the Drude formalism (Eq.2) to model the spectra of the films treated for times longer than 90 s (minimal exposure time used in our experiments). We associate this with a disordered character of defect states and/or chemical

functional groups generated at the walls of SWCNTs during plasma treatment. The corresponding distributions of effective lengths (distances between the introduced defects) of conducting pathways in the SWCNT network, of the values of charge carriers scattering rates γ_D and of crossover frequencies ν_{co} should inevitably affect the THz-FIR dynamics of the carriers. As a result, the analysis using Eq.2 with a *single* γ_D value, as was done above for the spectra of SWCNTs with different lengths, becomes inadequate for plasma-treated films. Due to the same reasons, we were not able to extract any quantitative information on the plasmonic resonance in these films. To obtain their broad-band THz-IR conductance spectra, we had to *formally* model the IR transmission coefficient and THz conductance spectra of the films with a set of several (three) artificial Lorentzians, Eqs.1. The results of such analysis are shown with dashed lines in Fig.2d,e,f.

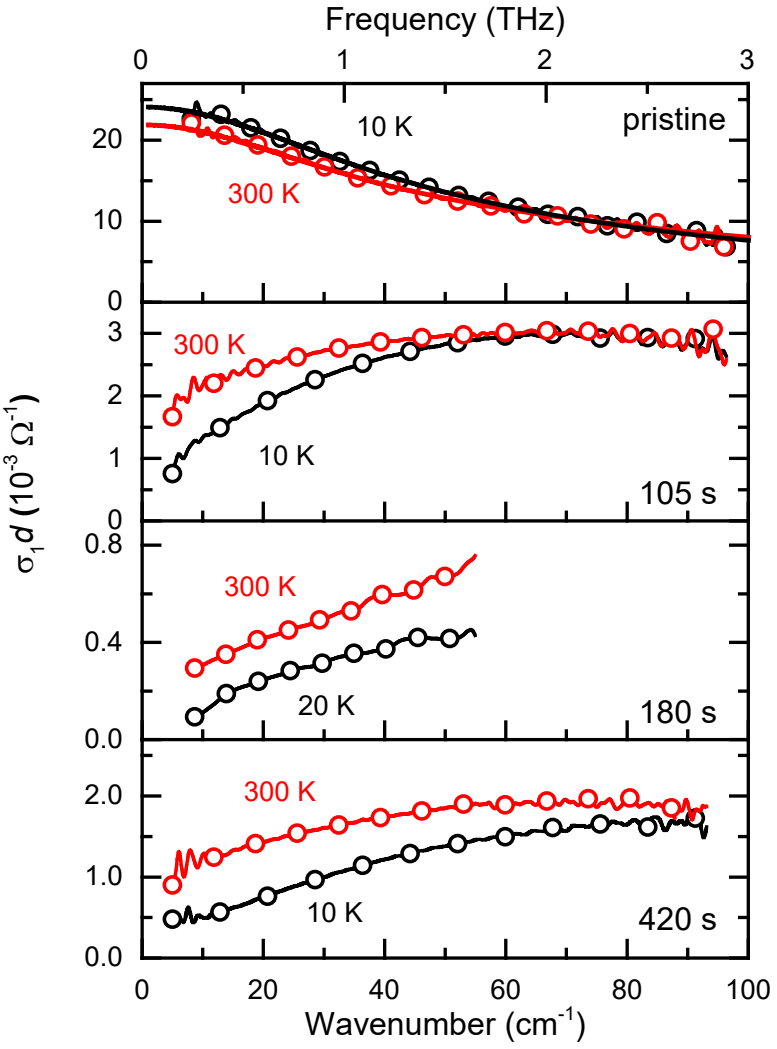

Fig.5. Terahertz spectra of the real part of conductance of SWCNT films composed of pristine SWCNTs (top panel) and SWCNTs treated with the plasma during different times as indicated (lower panels), measured at two different temperatures. Dots+lines show experimental data, solid lines in panel (a) indicate results of least-square fitting of spectra of SWCNT film composed of pristine SWCNTs using the Drude conductivity model (2) to

describe the response of delocalized carriers and Lorentzian expression (1) to describe plasmon resonance at around 100 cm^{-1}. Such fitting was not possible for plasma-treated films, as described in the text. The relatively larger conductance of the film that was irradiated for 420 s is due to the larger thickness of this film and to the correspondingly larger amount of pathways charge carriers can travel in the bulk of the film due to a larger number of resistive intertube contacts in parallel; as a result, the conductance is enhanced, while the effect of longer treatment fits the overall tendency of shifting of the peak position of the bump towards higher frequency.

Previously, we have demonstrated that exposing SWCNT films to oxygen plasma allows for tuning of their electronic properties that can help meet requirements in the production of broad-band infrared bolometers [10]. One of the main parameters responsible for the bolometric sensitivity of the films, the temperature coefficient of the static resistance (dc TCR), was shown to grow significantly after plasma irradiation and during lowering the temperature down to 100 K. The effect is connected with the enhancement of sensitivity to temperature variation of the dc sheet resistance R_{sq} of the films since thermal energy k_BT assists charge carriers in overcoming potential barriers generated during plasma exposure. From Fig.6, one can see that irradiating the films with plasma, as well as growing the films with shorter SWCNTs length, lead to similar effects also in ac case, *i.e.*, at THz frequencies: the absolute value of ac TCR grows up during cooling (Fig.6b,e). The absolute values of the obtained ac (0.3 THz) TCR at T=100 K (-0.1%...-0.2%/K for 105 s irradiation time; -0.2%...-0.3%/K for 0.3-1 μm long SWCNTs) are significantly smaller than the corresponding dc data of [10], ≈-3% for 75 s exposure time. The reason is that the sheet resistance gets higher at lower frequencies (Fig.6a,d) towards the dc limit where it is more effectively affected by heating or cooling: in the dc case, the charge carriers experience the finer structure of the localizing potential than in the ac case, the result being correspondingly larger temperature derivative of the dc resistance (*i.e.*, TCR) typically observed in disordered conductors [30,31]. This is demonstrated in Fig.6c,f, where the frequency dependence of ac TCR of both kinds of SWCNT films is shown. The ac TCR ceases to depend on frequency above 60 cm^{-1} (above 2 THz), where also the shielding effectiveness of SWCNT films weakens [5]. Both phenomena are caused by the diminishing role of the Drude charge carrier condensate in the ac response at frequencies $\nu > \gamma_D$ (according to Eq.2), where γ_D is in the range 50-100 cm^{-1} (*cf.* Fig.4a and the data obtained in [5,6]). It is worth noting that the ac TCR flattens at high plasma exposure times (longer than 100 s) and in films with short (below 1 μm) SWCNTs, see Fig.7; the same tendency towards saturation is noticed for dc TCR (see inset in Fig.4a in [10]). The flattening can be considered as a precursor of TCR reduction in the films that are exposed to plasma for a very long time when SWCNTs become severely damaged and lose their peculiar electric properties. We can thus say that treating the SWCNT films with oxygen plasma with the

used power of 100 W for times longer than ≈100 s or making films with SWCNT shorter than 1-0.3 μm will not lead to noticeable enhancement of TCR.

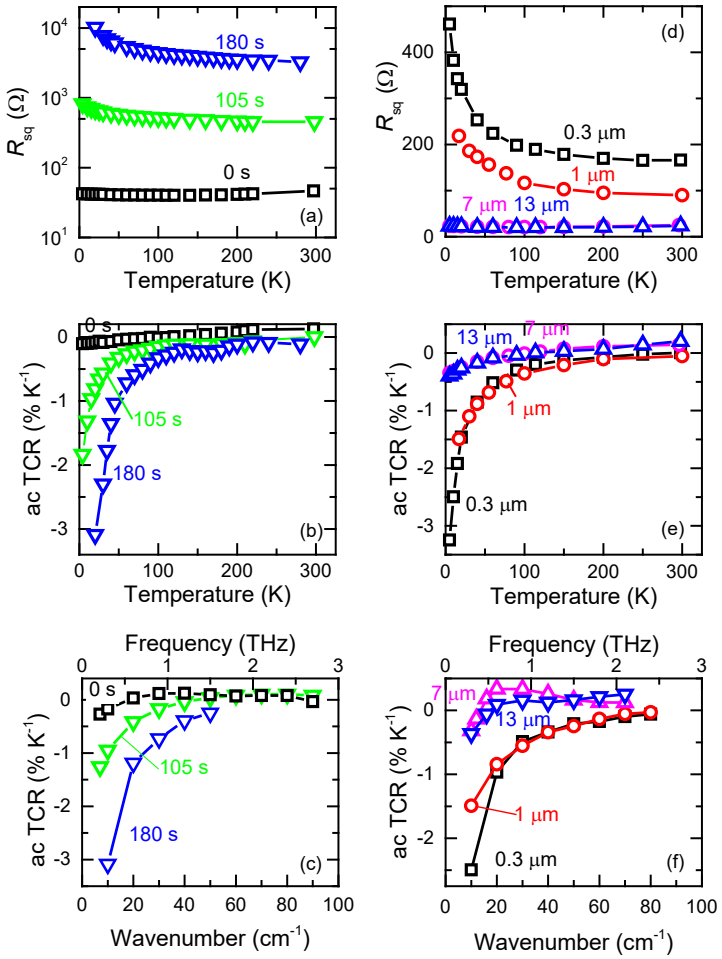

Fig.6. Temperature dependences of ac (0.3 THz) sheet resistance of SWCNT films exposed to plasma during different times (a) and composed of SWCNTs of different lengths (d). Panels b, c, e, f show temperature (b, e; frequency 0.3 THz) and frequency (c, f; temperature 10 K) dependences on corresponding temperature coefficients of films ac sheet resistance.

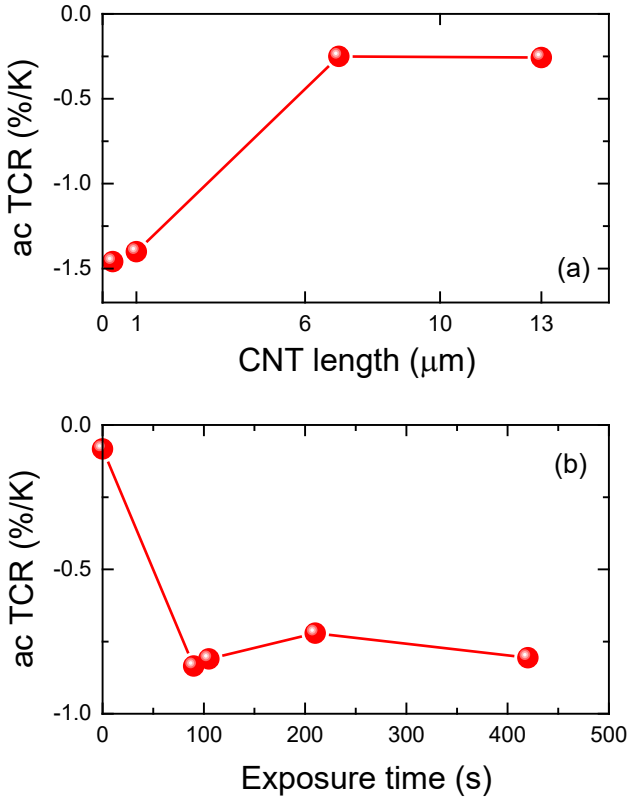

Fig.7. Dependences of temperature coefficient of ac (0.3 THz) resistance of SWCNT films on SWCNT average length (a) and plasma exposure time (b). Data were taken at temperature T=20 K.

4.Conclusions

We measured the temperature-dependent (temperatures 5-300 K) terahertz-infrared (frequencies 5-20 000 cm^{-1}) spectra of complex conductance of wafer-scale films composed of pristine and oxygen plasma-treated SWCNTs. For comparison, the same spectroscopic experiments were performed on films comprising SWCNTs with different lengths. We found that plasma irradiation had similar effects on the condensate of delocalized charge carriers as that observed in films with shorter SWCNTs. While THz-IR conductance spectra of films with pristine SWCNTs are well described by the Drude formalism with account taken of a plasmon-like resonance at 100 cm^{-1}, progressive exposure to plasma or growing films with shorter nanotubes' length lead to the gradual development of a gap-like feature in the terahertz response. We observed and qualitatively interpreted the SWCNT length dependence of the effective Drude parameters of the charge carriers (scattering rate and the dc conductance) and plasmonic resonance parameters (frequency position, oscillator strength, and damping). For films with nanotubes shorter than 1 μm, *i.e.* close to electrons mean free path and localization length, interaction of charge carriers with the nanotubes' edges was shown to additionally contribute to the carriers scattering rate and to the damping of plasmon resonance whose frequency position

increases in accordance with theoretical predictions. Due to the disordered character of induced defects, no quantitative information on the parameters of Drude condensate and plasmonic resonance in the plasma-treated films could be obtained. The temperature coefficient of ac resistance in both kinds of films was found to strongly depend on temperature and frequency. The absolute values of ac TCR increased for plasma-treated films with a longer treatment time and films with shorter nanotubes, but saturated for films with an exposure time longer than ≈100 s or composed by SWCNTs shorter than 1 μm.

Acknowledgements

The authors acknowledge Mogorychnaya A.V. for assistance with spectroscopic experiments. The research was supported by the Russian Science Foundation, grant RSF21-72-20050. D.S.K. and A.G.N. acknowledge Russian Foundation of Basic Research project No. 20-03-00804 (synthesis, characterization and plasma treatment of carbon nanotubes). A.P.T. acknowledges the EDUFI Fellowship (No. TM-19-11079) from the Finnish National Agency for Education and the Magnus Ehrnrooth Foundation (the Finnish Society of Sciences and Letters) for personal financial support.

References

[1] A.P. Tsapenko, A.E. Goldt, E. Shulga, Z.I. Popov, K.I. Maslakov, A.S. Anisimov, P.B. Sorokin, A.G. Nasibulin, Highly conductive and transparent films of HAuCl4-doped single-walled carbon nanotubes for flexible applications, Carbon N. Y. 130 (2018) 448–457. https://doi.org/10.1016/j.carbon.2018.01.016.

[2] M.G. Burdanova, A.P. Tsapenko, D.A. Satco, R. Kashtiban, C.D.W. Mosley, M. Monti, M. Staniforth, J. Sloan, Y.G. Gladush, A.G. Nasibulin, J. Lloyd-Hughes, Giant Negative Terahertz Photoconductivity in Controllably Doped Carbon Nanotube Networks, ACS Photonics. 6 (2019) 1058–1066. https://doi.org/10.1021/acsphotonics.9b00138.

[3] H. Xu, S.M. Anlage, L. Hu, G. Gruner, Microwave shielding of transparent and conducting single-walled carbon nanotube films, Appl. Phys. Lett. 90 (2007) 88–91. https://doi.org/10.1063/1.2734897.

[4] O. Hilt, H. Brom, M. Ahlskog, Localized and delocalized charge transport in single-wall carbon-nanotube mats, Phys. Rev. B - Condens. Matter Mater. Phys. 61 (2000) R5129–R5132. https://doi.org/10.1103/PhysRevB.61.R5129.

[5] B.P. Gorshunov, E.S. Zhukova, J.S. Starovatykh, M.A. Belyanchikov, A.K. Grebenko, A. V. Bubis, V.I. Tsebro, A.A. Tonkikh, D. V. Rybkovskiy, A.G. Nasibulin, E.I. Kauppinen,

E.D. Obraztsova, Terahertz spectroscopy of charge transport in films of pristine and doped single-wall carbon nanotubes, Carbon N. Y. 126 (2018) 544–551. https://doi.org/10.1016/j.carbon.2017.10.072.

[6] E.S. Zhukova, A.K. Grebenko, A. V Bubis, A.S. Prokhorov, M.A. Belyanchikov, A.P. Tsapenko, E.P. Gilshteyn, D.S. Kopylova, Y.G. Gladush, A.S. Anisimov, V.B. Anzin, A.G. Nasibulin, B.P. Gorshunov, Terahertz-infrared electrodynamics of single-wall carbon nanotube fi lms, (2017).

[7] D.S. Kopylova, D.A. Satco, E.M. Khabushev, A. V. Bubis, D. V. Krasnikov, T. Kallio, A.G. Nasibulin, Electrochemical enhancement of optoelectronic performance of transparent and conducting single-walled carbon nanotube films, Carbon N. Y. 167 (2020) 244–248. https://doi.org/10.1016/j.carbon.2020.05.103.

[8] K.K. Kim, S.M. Yoon, H.K. Park, H.J. Shin, S.M. Kim, J.J. Bae, Y. Cui, J.M. Kim, J.Y. Choi, Y.H. Lee, Doping strategy of carbon nanotubes with redox chemistry, New J. Chem. 34 (2010) 2183–2188. https://doi.org/10.1039/c0nj00138d.

[9] V.Y. Iakovlev, Y.A. Sklyueva, F.S. Fedorov, D.P. Rupasov, V.A. Kondrashov, A.K. Grebenko, K.G. Mikheev, F.Z. Gilmutdinov, A.S. Anisimov, G.M. Mikheev, A.G. Nasibulin, Improvement of optoelectronic properties of single-walled carbon nanotube films by laser treatment, Diam. Relat. Mater. 88 (2018) 144–150. https://doi.org/10.1016/j.diamond.2018.07.006.

[10] D.S. Kopylova, F.S. Fedorov, A.A. Alekseeva, E.P. Gilshteyn, A.P. Tsapenko, A. V. Bubis, A.K. Grebenko, Z.I. Popov, P.B. Sorokin, Y.G. Gladush, A.S. Anisimov, A.G. Nasibulin, Holey single-walled carbon nanotubes for ultra-fast broad-band bolometers, Nanoscale. 10 (2018) 18665–18671. https://doi.org/10.1039/c8nr05925j.

[11] P.C.P. Watts, N. Mureau, Z. Tang, Y. Miyajima, J. David Carey, S.R.P. Silva, The importance of oxygen-containing defects on carbon nanotubes for the detection of polar and non-polar vapours through hydrogen bond formation, Nanotechnology. 18 (2007). https://doi.org/10.1088/0957-4484/18/17/175701.

[12] J.A. Robinson, E.S. Snow, Ş.C. Bădescu, T.L. Reinecke, F.K. Perkins, Role of defects in single-walled carbon nanotube chemical sensors, Nano Lett. 6 (2006) 1747–1751. https://doi.org/10.1021/nl0612289.

[13] M. Mahjouri-Samani, Y.S. Zhou, X.N. He, W. Xiong, P. Hilger, Y.F. Lu, Plasmonic-enhanced carbon nanotube infrared bolometers, Nanotechnology. 24 (2013).

https://doi.org/10.1088/0957-4484/24/3/035502.

[14] R.R. Hartmann, J. Kono, M.E. Portnoi, Terahertz science and technology of carbon nanomaterials, Nanotechnology. 25 (2014). https://doi.org/10.1088/0957-4484/25/32/322001.

[15] C. Woong Jang, Y. Tae Byun, D. Ha Woo, S. Lee, Y. Min Jhon, Oxygen plasma post process to obtain consistent conductance of carbon nanotubes in carbon nanotube field-effect transistors, Appl. Phys. Lett. 101 (2012). https://doi.org/10.1063/1.4762829.

[16] S. Yeo, C. Choi, C.W. Jang, S. Lee, Y.M. Jhon, Sensitivity enhancement of carbon nanotube based ammonium ion sensors through surface modification by using oxygen plasma treatment, Appl. Phys. Lett. 102 (2013). https://doi.org/10.1063/1.4793482.

[17] T. Morimoto, K. Kobashi, T. Okazaki, Carbon Nanotube Length Distribution Estimation by One-Dimensional Plasmon Resonance for Solid-State Samples, J. Phys. Chem. C. (2021). https://doi.org/10.1021/acs.jpcc.1c04539.

[18] T. Morimoto, S. Joung, T. Saito, D.N. Futaba, K. Hata, Length-Dependent Plasmon Resonance in Single-Walled Carbon, (2014) 9897–9904.

[19] P. Karlsen, M. V. Shuba, C. Beckerleg, D.I. Yuko, P.P. Kuzhir, S.A. Maksimenko, V. Ksenevich, H. Viet, A.G. Nasibulin, R. Tenne, E. Hendry, Influence of nanotube length and density on the plasmonic terahertz response of single-walled carbon nanotubes, J. Phys. D. Appl. Phys. 51 (2018). https://doi.org/10.1088/1361-6463/aa96ef.

[20] A. Kaskela, A.G. Nasibulin, M.Y. Timmermans, B. Aitchison, A. Papadimitratos, Y. Tian, Z. Zhu, H. Jiang, D.P. Brown, A. Zakhidov, E.I. Kauppinen, Aerosol-synthesized SWCNT networks with tunable conductivity and transparency by a dry transfer technique, Nano Lett. 10 (2010) 4349–4355. https://doi.org/10.1021/nl101680s.

[21] H. Kataura, Y. Kumazawa, Y. Maniwa, I. Umezu, S. Suzuki, Y. Ohtsuka, Y. Achiba, Optical properties of single-wall carbon nanotubes, Synth. Met. 103 (1999) 2555–2558. https://doi.org/10.1016/S0379-6779(98)00278-1.

[22] Y. Troitskii, Dispersed Metallic Films, Institute of Physics USSR Academy of Sciences, Kiev, 1972.

[23] M. Born, Principles of optics, 6th ed., Pergamon Press, 1980.

[24] A. Sokolov, Optical Properties of Metals, American Elsevier, New York, 1967.

[25] M. Dressel, Electrodynamics of Solids, Cambridge University Press, Cambridge, 2002.

[26] L.C. Venema, J.W.G. Wildöer, J.W. Janssen, S.J. Tans, H.L.J. Temminck Tuinstra, L.P. Kouwenhoven, C. Dekker, Imaging electron wave functions of quantized energy levels in carbon nanotubes, Science (80-.). 283 (1999) 52–55. https://doi.org/10.1126/science.283.5398.52.

[27] M.J. Rice, J. Bernasconi, Interrupted strand model for quasi one dimensional metals, J. Phys. F Met. Phys. 3 (1973) 55–66. https://doi.org/10.1088/0305-4608/3/1/016.

[28] A.A. Ignatov, Field and Frequency-dependent Dilectric Constant of Quasi-one-dimensional Semiconductors, Solid State Commun. 41 (1982) 495–497.

[29] A.A. Gogolin, Electron localization and hopping conductivity in one-dimensional disordered systems, Phys. Rep. 86 (1982) 1–53. https://doi.org/10.1016/0370-1573(82)90069-2.

[30] N.F. Mott, E. Davis, Electronic Processes in Noncrystalline Solids, Oxford University Press, London, 1971.

[31] T.B. Schrøder, J.C. Dyre, Scaling and universality of ac conduction in disordered solids, Phys. Rev. Lett. 84 (2000) 310–313. https://doi.org/10.1103/PhysRevLett.84.310.

[32] T. Nakanishi, T. Ando, Optical Response of Finite-Length Carbon Nanotubes, J. Phys. Soc. Japan. 78 (2009) 114708. https://doi.org/10.1143/jpsj.78.114708.